

# Modulation Symbol Pulse Shaping Transceiver for Affine Frequency Division Multiplexing

Haojian Zhang, *Graduate Student Member, IEEE*, Jiayan Yang,  
Tingting Zhang, *Member, IEEE*, Xu Zhu, *Senior Member, IEEE*

**Abstract**—The recently proposed affine frequency division multiplexing (AFDM) waveform can adjust the time-frequency diversity gain by tuning chirp-rate parameter. Therefore, it is a candidate waveform in doubly-selective channels. This letter reveals that the modulation-symbol-domain shaping pulse of AFDM is generated by a convolution-like operation between the time-domain and frequency-domain shaping pulses, indicating that the modulation-symbol-domain pulse shaping of AFDM can be achieved by separately shaping in the time domain and frequency domain. Based on this, this letter presents an AFDM modulation-symbol-domain pulse shaping transceiver which has an ability to achieve the Nyquist pulse shaping, and provides the corresponding input-output relationship. Numerical results demonstrate the effectiveness of the proposed transceiver in improving the channel sparsity and pilot-to-data interference.

**Index Terms**—Affine frequency division multiplexing, pulse shaping, doubly-selective channels, wireless communications.

## I. INTRODUCTION

IN recent years, various modulation waveforms have been proposed for the wireless communications in doubly-selective channels [1]-[5]. Among these waveforms, the chirp-based affine frequency division multiplexing (AFDM) can adjust the modulation symbol dispersions in doubly-selective channel through using channel-customized chirp-rate parameter, thereby obtaining time-frequency diversity gain [5]-[7]. AFDM has become a candidate waveform under doubly-selective channels, and multiple studies have been conducted, such as channel estimation, channel equalization, multiple input multiple output, and multiple access [8]-[14].

Pulse shaping is an important step in digital signal processing, which adjusts the tail attenuation features of discrete samples in the continuous domain at the cost of potentially increasing the bandwidth of the dual domain by Fourier transform. For instance, time-domain pulse shaping can rapidly attenuate digital signals in the time domain, thereby reducing the time-domain guard interval between the two adjacent signals for avoiding inter-symbol interference. For wireless communication signals, pulse shaping in the modulation symbol domain also plays an important role, as it determines the sparsity of the modulation-symbol-domain channel, and the interference between modulation symbols after passing through the

channel. The research in [14] reveals the significance of inter-pulse interference, which influences the accuracy of channel estimation, and inter-region interference, which characterizes the pilot-to-data interference, in the embedded-pilot-based AFDM waveform. Moreover, the research in [14] verifies that modulation-symbol-domain pulse shaping can improve the performance of AFDM via direct time-domain transmission and reception windowing. However, the analysis of the pulse shaping mechanism in [14] is still insufficient, as it does not clearly indicate the coupling from time-domain shaping pulses in the input-output relationship of AFDM. Moreover, the proposed direct time-domain windowing method cannot achieve Nyquist pulse shaping, which remains to be improved in shaping flexibility.

By conducting a further analysis of the input-output relationship, this letter reveals that the modulation-symbol-domain (also known as the discrete affine Fourier transform domain) shaping pulse of AFDM is generated by a convolution-like operation between the time-domain and frequency-domain shaping pulses, indicating that the modulation-symbol-domain pulse shaping of AFDM can be achieved by separately shaping in the time domain and frequency domain. Based on this, this letter presents an AFDM modulation-symbol-domain pulse shaping transceiver and provides the corresponding input-output relationship. The proposed method can adjust the pulse width of the modulation symbol domain by adjusting the cyclic prefix and postfix, improving the flexibility of AFDM pulse shaping. Numerical results demonstrate the effectiveness of the proposed transceiver in improving the channel sparsity and pilot-to-data interference.

## II. PULSE SHAPING ANALYSIS IN AFDM

This section provides the derivation of input-output relationship and the derivative pulse shaping analysis in AFDM waveform.

### A. Time-domain signal model

The receipt baseband signal can be express as

$$s_R(t) = g_{t,R}(t) * \left( \sum_{p=0}^{P-1} \alpha_p s_T(t - \tau_p(t)) e^{-j2\pi f_c \tau_p(t)} \right) \quad (1)$$

where  $*$  denotes the linear convolution operator.  $\alpha_p \in \mathbb{C}$  and  $\tau_p \in \mathbb{R}$  denote the path gain and time-varying delay of the  $p$ -th path in propagation channel, respectively.  $g_{t,R}(t)$  denotes the

The source codes for the simulations in this paper will be released on GitHub. The corresponding URL will be provided in the subsequent version of manuscript.

The authors are with the School of Information Science and Technology, Harbin Institute of Technology (Shenzhen), Shenzhen, 518055, China. (e-mail: zhanghaojian@hotmail.com; jiayanyoung@gmail.com; zhangtt@hit.edu.cn; xuzhu@ieec.org)

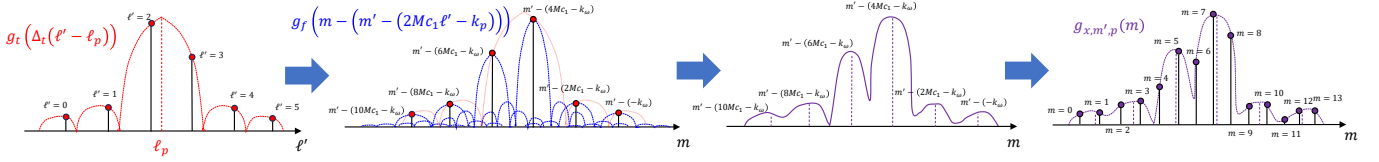


Fig. 1. Illustration of the pulse shaping in AFDM, from time-domain pulse  $g_t$  and frequency-domain pulse  $g_f$  to modulation-symbol-domain pulse  $g_x$ .

time-domain receipt shaping pulse.  $s_T(t)$  denotes the transmit baseband signal, given by

$$s_T(t) = \sum_{\ell'=-L}^{M-1} s[\ell'] g_{t,T}(t - \Delta_t \ell') \quad (2)$$

where  $\Delta_t = 1/(M\Delta_f)$  denotes the baseband sampling time interval.  $\Delta_f$  and  $M$  denote the subcarrier interval and overall subcarrier number, respectively.  $s[\ell']$  denotes the transmit baseband digital signal with length  $M + L$ , where  $L$  denotes the prefix length of the waveform.  $g_{t,T}(t)$  is the time-domain transmit shaping pulse. Introduce the following common assumptions based on Eq. (1):

1) The delay variation is considered as a linear model within the duration of baseband signal, that is,

$$\tau_p(t) = \tau_p + \gamma_p t \quad (3)$$

2) The scaling effect of  $g_{t,T}(t)$  caused by time-varying path delay  $\tau_p(t)$  can be ignored within the duration of baseband signal, that is,

$$g_{t,T}(t - \Delta_t \ell' - \tau_p(t)) \approx g_{t,T}(t - \Delta_t \ell' - \tau_p) \quad (4)$$

3) The shaping mismatch caused by  $e^{-j2\pi f_c \tau_p(t)}$  between the transmit and receipt shaping pulses can be ignored within the duration of baseband signal, that is,

$$\begin{aligned} g_{t,R}(t) & * \left( g_{t,T}(t - \Delta_t \ell' - \tau_p) e^{-j2\pi f_c \tau_p(t)} \right) \\ & \approx (g_{t,R}(t) * g_{t,T}(t - \Delta_t \ell' - \tau_p)) e^{-j2\pi f_c \tau_p(t)} \\ & = g_t(t - \Delta_t \ell' - \tau_p) e^{-j2\pi f_c \tau_p(t)} \end{aligned} \quad (5)$$

where  $g_t(t) = g_{t,T}(t) * g_{t,R}(t)$  denotes the overall time-domain shaping pulse.

Thus,  $s_R(t)$  can be further express as

$$\begin{aligned} s_R(t) & = \sum_{p=0}^{P-1} \underbrace{\alpha_p e^{-j2\pi f_c \tau_p}}_{h_p} \\ & \times \left( \sum_{\ell'=-L}^{M-1} s[\ell'] g_t(t - \Delta_t \ell' - \tau_p) e^{j2\pi \nu_p t} \right) \end{aligned} \quad (6)$$

where  $\nu_p = -f_c \gamma_p$  denotes the doppler frequency of the  $p$ -th path. The third assumption establishes for  $\nu_p \ll M\Delta_f$ . Sampling the received signal  $s_R(t)$  at the time interval of  $\Delta_t$  while removing the prefix, the receipt baseband digital signal

$r[\ell]$  is obtained, given by

$$\begin{aligned} r[\ell] & = \sum_{p=0}^{P-1} h_p e^{j\frac{2\pi}{M} k_p \ell} \left( \sum_{\ell'=-L}^{M-1} s[\ell'] g_t(\Delta_t(\ell - \ell' - \ell_p)) \right) \\ & = \sum_{p=0}^{P-1} \sum_{\ell'=\ell-M+1}^{\ell+L} h_p g_t(\Delta_t(\ell' - \ell_p)) s[\ell - \ell'] e^{j\frac{2\pi}{M} k_p \ell} \end{aligned} \quad (7)$$

where  $0 \leq \ell < M$ ,  $\ell_p = \tau_p/\Delta_t \in \mathbb{R}$ ,  $k_p = \nu_p/\Delta_f \in \mathbb{R}$ . Due to the tail attenuation property of  $g_t(t)$ , there is

$$g_t(t) = 0, \quad |t| > (G\Delta_t)/2 \quad (8)$$

Thus, the receipt baseband digital signal  $r[\ell]$  is further expressed as

$$r[\ell] = \sum_{p=0}^{P-1} \sum_{\ell'=\lfloor \ell_p \rfloor - G/2}^{\lceil \ell_p \rceil + G/2} h_p g_t(\Delta_t(\ell' - \ell_p)) s[\ell - \ell'] e^{-j\frac{2\pi}{M} k_p \ell} \quad (9)$$

where  $0 \leq \ell < M$ .

### B. Input-output relationship in AFDM

The transmit baseband digital signal  $s[\ell']$  of AFDM waveform is given by

$$s[\ell'] = \frac{1}{\sqrt{M}} \sum_{m'=0}^{M-1} x[m'] e^{j2\pi(c_1 \ell'^2 + \frac{m' \ell'}{M} + c_2 m'^2)}, \quad -L \leq \ell' < M \quad (11)$$

where  $x[m']$  denotes the  $m'$ -th transmit modulation symbol. It is seen that AFDM is a sort of chirp-based modulation waveform. At receiver side, the AFDM receipt modulation symbols  $y[m]$  are given by

$$y[m] = \frac{1}{\sqrt{M}} \sum_{\ell=0}^{M-1} r[\ell] e^{-j2\pi(c_1 \ell^2 + \frac{m \ell}{M} + c_2 m^2)}, \quad 0 \leq m < M \quad (12)$$

Substituting Eqs. (9) and (11) into Eq. (12), the modulation-symbol-domain input-output relationship of AFDM is obtained, given by Eq. (10), where  $g_f(m)$  given by Eq. (13) is a sinc-like function, and  $[\mathbf{H}]_{m,m'}$  is the entry of the  $m$ -th row and  $m'$ -th column in channel matrix.

$$g_f(m) = \frac{\sin(\pi m)}{M \sin(\frac{\pi}{M} m)} e^{-j\pi \frac{(M-1)}{M} m} \quad (13)$$

From Eq. (10), it can be seen that the modulation symbols  $x[m']$  have a convolution-like operation with the channel response. This implies that a single modulation symbol will

$$\begin{aligned}
y[m] &= \frac{1}{\sqrt{M}} \sum_{\ell=0}^{M-1} \sum_{p=0}^{P-1} \sum_{\ell'=\lfloor \ell_p \rfloor - G/2}^{\lceil \ell_p \rceil + G/2} h_p g_t(\Delta_t(\ell' - \ell_p)) \frac{1}{\sqrt{M}} \sum_{m'=0}^{M-1} x[m'] e^{j2\pi \left( c_1(\ell - \ell')^2 + \frac{m'(\ell - \ell')}{M} + c_2 m' \ell' \right)} e^{-j2\pi \left( c_1 \ell^2 + \frac{m\ell}{M} + c_2 m^2 \right)} \\
&= \sum_{m'=0}^{M-1} x[m'] \underbrace{\left( e^{j2\pi c_2(m'^2 - m^2)} \sum_{p=0}^{P-1} \sum_{\ell'=\lfloor \ell_p \rfloor - G/2}^{\lceil \ell_p \rceil + G/2} h_p e^{j\frac{2\pi}{M}(Mc_1 \ell'^2 - m' \ell')} g_t(\Delta_t(\ell' - \ell_p)) g_f(m - (m' - (2Mc_1 \ell' - k_p))) \right)}_{g_{x,m',p}(m)} \quad (10) \\
&\quad \underbrace{\hspace{10em}}_{[\mathbf{H}]_{m,m'}}
\end{aligned}$$

disperse into multiple weighted replicas after passing the channel, where the positions of the dispersed replicas are related to both path delays and Dopplers. Therefore, AFDM has the potential to obtain sufficient time-frequency diversity gain when the delay and Doppler parameters of different paths leads the channel responses of these paths sufficiently separated in the modulation symbol domain.

### C. Pulse Shaping Mechanism in AFDM

In Eq. (10),  $g_{x,m',p}(m)$  denotes the  $p$ -th path response from the  $m'$ -th transmit modulation symbol at receiver side. The magnitude envelop of  $g_{x,m',p}(m)$  is decided by the modulation-symbol-domain shaping pulse. The expression of  $g_{x,m',p}(m)$  in Eq. (10) shows that the modulation-symbol-domain shaping pulse is generated by a convolution-like operation between the time-domain shaping pulse  $g_t(t)$  and frequency-domain shaping pulse  $g_f(m)$ . Fig. 1 presents the process to obtain the modulation-symbol-domain pulse  $g_{x,m',p}(m)$  from the time-domain pulse  $g_t(t)$  and frequency-domain pulse  $g_f(m)$ . Firstly, the delayed time-domain pulse  $g_t(\Delta_t(\ell' - \ell_p))$  does a scale transformation with the factor of  $-2Mc_1$  and a followed circular shift of  $k_p + m'$ . Next, each of the sampled time-domain pulse taps modulates with the frequency-domain pulse  $g_f(m)$ . Finally, the modulation-symbol-domain shaping pulse  $g_{x,m',p}(m)$  is formed after superposition and resampling on the  $m$  dimension. From the generation of  $g_{x,m',p}(m)$ , it is inferred that the pulse tail in the modulation symbol domain is jointly suppressed by the time and frequency domain shaping pulses.

## III. PROPOSED PULSE SHAPING METHOD FOR AFDM

This section provides a modulation-symbol-domain pulse shaping method and the corresponding input-output relationship for AFDM waveform.

### A. Pulse shaping method

Based on the analysis in Sec. II-C, this section presents an AFDM modulation symbol pulse shaping method illustrated in Fig. 2<sup>1</sup>. Compared with the approach in [14], the proposed method allows more flexible pulse-width configuration of the time and frequency domain shaping pulses (e.g., whether to satisfy the Nyquist criterion in the frequency domain).

<sup>1</sup>In practical zero-intermediate-frequency systems, time-domain pulse shaping is usually performed in the upsampled digital domain. For clarity of presentation, Fig. 2 depicts the time-domain pulse shaping in the analog domain.

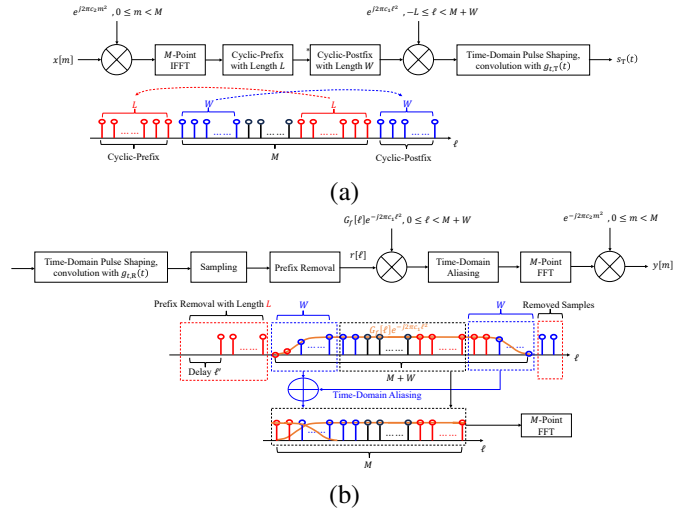


Fig. 2. Proposed modulation symbol pulse shaping method for AFDM at (a) transmitter side, (b) receiver side.

Time-domain pulse shaping is implemented through matched filtering at the transmitter and receiver as the general realization in practical systems, while frequency-domain pulse shaping is achieved by time-domain windowing and aliasing at receiver side. The combination of these two procedures realizes the pulse shaping in the modulated symbol domain for AFDM waveform. The interpolation of a cyclic postfix together with the aliasing operation provides an adjustment margin for pulse-width in the frequency domain. Note that if the Nyquist shaping criterion is desired to be satisfied, the presented shaping method incurs shaping overhead in the time-frequency domain. When raised-cosine pulses are adopted in both domains, the overhead coefficients correspond to the roll-off factors in the respective domains.

### B. Corresponding input-output relationship

The forms of the AFDM transmit baseband signal  $s[\ell']$  and receipt baseband signal  $r[\ell]$  corresponding to the shaping method shown in Fig. 2 are consistent with Eq. (11) and Eq. (9), respectively, except that the range of the time indexes  $\ell'$  and  $\ell$  are different, that is,  $-L \leq \ell' < M + W$  and  $0 \leq \ell < M + W$  in the proposed method. Moreover, the

$$\begin{aligned}
y[m] &= \frac{1}{\sqrt{M}} \sum_{\ell=0}^{M+W-1} G_f[\ell] r[\ell] e^{-j2\pi(c_1 \ell^2 + \frac{m\ell}{M} + c_2 m^2)} \\
&= \frac{e^{-j2\pi c_2 m^2}}{\sqrt{M}} \left( \sum_{\ell=0}^{M-1} G_f[\ell] r[\ell] e^{-j2\pi(c_1 \ell^2 + \frac{m\ell}{M})} + \sum_{\ell'=0}^{W-1} G_f[\ell'+M] r[\ell'+M] e^{-j2\pi(c_1(\ell'+M)^2 + \frac{m(\ell'+M)}{M})} \right) \\
&= \frac{e^{-j2\pi c_2 m^2}}{\sqrt{M}} \sum_{\ell=0}^{M-1} \underbrace{\left( G_f[\ell] r[\ell] e^{-j2\pi c_1 \ell^2} + G_f[\ell+M] r[\ell+M] e^{-j2\pi c_1(\ell+M)^2} \right)}_{\text{Time-Domain Aliasing, } G_f[\ell]=r[\ell]=0 \text{ for } \ell \geq M+W} e^{-j\frac{2\pi}{M} m \ell}
\end{aligned} \tag{14}$$

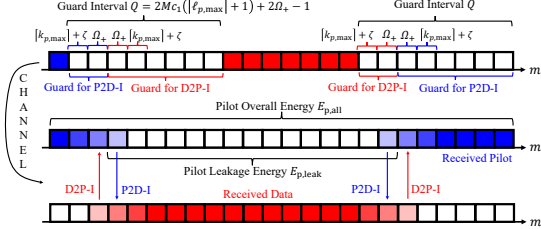


Fig. 3. Illustration of the embedded pilot for simulations (P2D-I: pilot-to-data interference, D2P-I: data-to-pilot interference).

receipt modulation symbols  $y[m]$  are given by

$$\begin{aligned}
y[m] &= \frac{1}{\sqrt{M}} \sum_{\ell=0}^{M+W-1} G_f[\ell] r[\ell] e^{-j2\pi(c_1 \ell^2 + \frac{m\ell}{M} + c_2 m^2)} \\
&, \quad 0 \leq m < M
\end{aligned} \tag{15}$$

From  $s[\ell']$ ,  $r[\ell]$  and Eq. (15), the input-output relationship of the proposed shaping method is exactly the same as the final form of Eq. (10), with the difference of

$$\begin{aligned}
&g_f(m - (m' - (2Mc_1 \ell' - k_p))) \\
&= \frac{1}{M} \sum_{\ell=0}^{M+W-1} G_f[\ell] e^{-j\frac{2\pi}{M}(m - (m' - (2Mc_1 \ell' - k_p)))\ell}
\end{aligned} \tag{16}$$

Additionally, Eq. (14) presents the relationship between  $y[m]$  and time-domain aliasing operation.

#### IV. NUMERICAL RESULTS

This section presents the numerical validations of the proposed shaping method in terms of the improvements of channel sparsity and pilot-to-data interference using an embedded pilot located at  $m' = 0$  as shown in Fig. 3. The time-domain Nyquist shaping pulse is decomposed into two root-raised-cosine pulses at both the transmitter and receiver with the roll-off factor of  $\alpha_t$ . The subcarrier number and length of cyclic-prefix are set to  $M = 4096$  and  $L = 288$ , respectively, common in 5G configurations. The chirp-rate parameters  $c_1$  and  $c_2$  are set to  $\frac{2([k_{p,\max}] + \zeta) + 1}{2M}$  and 0, respectively [5].  $\zeta$  is a parameter used to adjust the separation degree between channel paths considering the off-grid Doppler effect. The extended guard interval  $\Omega_+$  is adjustable for the tolerance for the interference caused by off-grid delay and Doppler. In the simulations, time-domain pulse shaping is implemented in the digital domain after upsampling, where the upsampling factor and filter order are set to 8 and 1024, respectively. In particular, when a Nyquist frequency-domain pulse shaping

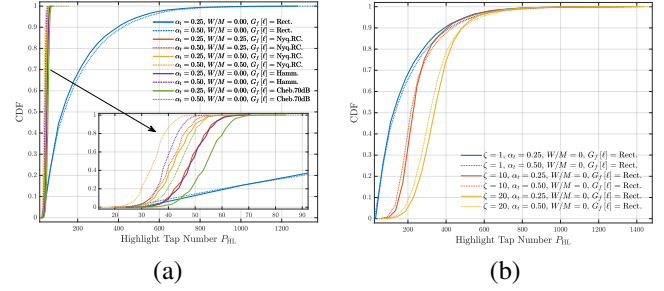


Fig. 4. Cumulative distribution functions of the highlight tap numbers  $P_{HL}$  (the lower is better) for (a) using different shaping pulses with  $\eta = -30\text{dB}$  and  $\zeta = 1$ , (b) using rectangular window shaping with different  $\zeta$ .

with the roll-off factor of  $\alpha_f$  is adopted, the length of cyclic-postfix  $W$  is set to  $\lceil \alpha_f M \rceil$ . There are  $P = 10$  paths in the simulated channels, where the path gains  $h_p$  follow the complex Gaussian distribution of  $\mathcal{CN}(0, 1)$ , the path delays  $\ell_p$  follow the uniform distribution of  $\mathcal{U}[0, \ell_{p,\max}]$  and  $\ell_{p,\max} = 10$ , and the path Dopplers  $k_p = k_{p,\max} \cos \theta_p$  and  $k_{p,\max} = 1$ ,  $\theta_p \sim \mathcal{U}[-\pi, \pi]$ . The number of Monte Carlo tests is set to  $10^4$ . In the following figures, ‘‘Rect.’’, ‘‘Nyq.RC.’’, ‘‘Hamm.’’ and ‘‘Cheb.70dB’’ denote the rectangular, Nyquist-raised-cosine, Hamming and Chebyshev (-70dB sidelobe) pulse shaping  $G_f[\ell]$ , respectively, in the frequency domain.

##### A. Improvement of the channel sparsity

This subsection uses the number of ‘‘highlighted tap number  $P_{HL}$ ’’ in the receipt modulation symbols  $y_m$  as the criterion for evaluating the channel sparsity improvement under different shaping pulses. The metric  $P_{HL}$  corresponds to the number of power-dominated elements of  $y[m]$  beyond which the residual power becomes less than  $\eta$  times the total received power of  $y[m]$ . The parameters  $\zeta$  and  $\Omega_+$  are set to 1 and 20, respectively. The cumulative distribution function (CDF) of the simulated  $P_{HL}$  in Fig. 4-(a) shows that the use of Nyquist RC time-frequency shaping with higher roll-off factors can significantly enhance channel sparsity, while the cost is the increasing of the time-frequency overhead. However, Fig. 4-(a) shows two counterintuitive issues:

1) When frequency-domain rectangular shaping is used, the increasing of time-domain roll-factor  $\alpha_t$  results in the slightly degradation of channel sparsity. This is caused by the incoherent superposition of the overlapped path responses resultant from fractional Doppler. A smaller  $\alpha_t$  reduces the power difference between adjacent samples of  $g_t(\Delta_t(\ell' - \ell_p))$ . These taps are further overlapped after being modulated with the high-sidelobe frequency-domain shaping pulse  $g_f(m)$  in the

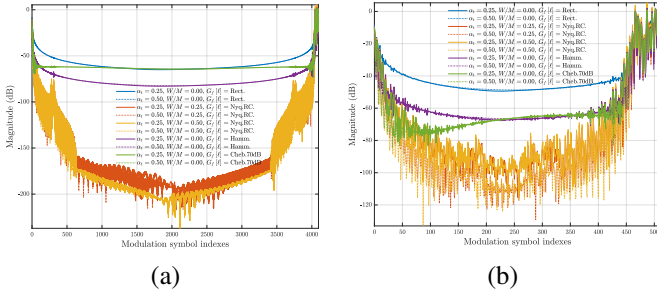


Fig. 5. Magnitude profiles of one realization of  $y[m]$  using different shaping pulses with the subcarrier number of (a)  $M = 4096$ , (b)  $M = 512$ .

modulation symbol domain. After the incoherent superposition in the modulation domain, the power variation of final path response may become more dramatic, resulting in some low-power elements in  $y[m]$ . This phenomenon results in slightly better channel sparsity in smaller  $\alpha_t$ . On the other hand, if the distance between the samples of  $g_t(\Delta_t(\ell' - \ell_p))$  is increased to alleviate the incoherent superposition effect in the modulation symbol domain, a higher  $\alpha_t$  can be beneficial for channel sparsity. Fig. 4(b) provides the corresponding demonstration, where the distance of the samples of  $g_t(\Delta_t(\ell' - \ell_p))$  increases in the modulation symbol domain via increasing  $\zeta$ . And also, the incoherent superposition effect can be alleviated via decreasing the sidelobes of  $g_f(m)$  which is already demonstrated in Fig. 4(a) while the sparsity degradation caused by separated sidelobes.

2) The frequency-domain Chebyshev shaping results in the degradation of channel sparsity compared with the Hamming shaping which has higher proximal sidelobes. This is caused by the constant-sidelobe feature of the Chebyshev shaping. As shown in Fig. 5(a), the far sidelobes using the Hamming shaping continue to attenuate, and become lower than those using the Chebyshev shaping when a large subcarrier number is adopted. Meanwhile, the main energy of the path response using the Hamming shaping is more concentrated. This allows to achieve the same energy ratio with fewer elements of  $y[m]$  using Hamming shaping.

### B. Improvement of the pilot-to-data interference

This section uses average energy leakage ratio  $\frac{E_{p,leak}}{E_{p,all}}$  to evaluate the impact of different shaping pulses on pilot-to-data interference, where the range of  $E_{p,leak}$  and  $E_{p,all}$  can be seen in Fig. 3. The parameter  $\zeta$  is set to 1. From Fig. 6(a), it is seen that increasing  $\alpha_t$  can significantly reduce the pilot guard overhead  $\Omega_+$ . Meanwhile, the use of Nyquist RC shaping in the frequency domain can significantly reduce the energy leakage floor, thereby achieving lower pilot-to-data interference under a given  $\Omega_+$ . This is due to the continuous and rapid attenuation features of the far sidelobes in the Nyquist RC shaping as shown in Fig. 5(a). Additionally, in Fig. 6(a), the performance curves with the frequency-domain roll-off factors of 0.25 and 0.5 almost overlap. Similarly, Chebyshev shaping with lower near sidelobes performs worse than Hamming shaping in terms of energy leakage floor. The reason is that the Chebyshev shaping have higher far sidelobes

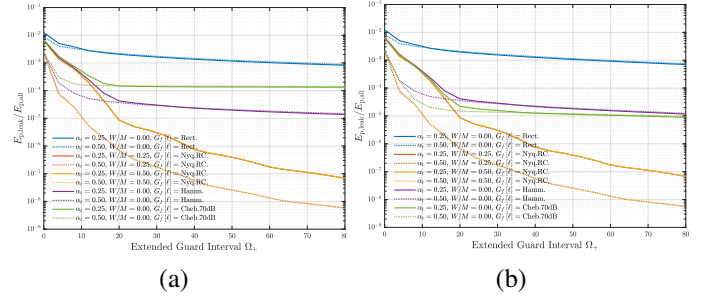


Fig. 6. Average leakage energy ratio  $\frac{E_{p,leak}}{E_{p,all}}$  under different extended guard intervals  $\Omega_+$  with the subcarrier number of (a)  $M = 4096$ , (b)  $M = 512$ .

than Hamming shaping when the subcarrier number is large. As a comparison, Fig. 6(b) provides the evaluation results for the case with the subcarrier number of 512, indicating that Chebyshev shaping has a lower leakage level than Hamming shaping at this time. From Fig. 5(b), it is seen that the far sidelobes of Chebyshev shaping are always lower than Hamming shaping under a smaller subcarrier number.

## V. CONCLUSIONS

This letter studies the input-output relationship of AFDM waveform, showing the coupling between time-domain, frequency-domain, and modulation-symbol-domain shaping pulses. It points out that modulation-symbol-domain pulse shaping in AFDM can be achieved by separately shaping in the time domain and frequency domain. Based on this analysis conclusion, a modulation-symbol-domain pulse shaping method which can achieve the Nyquist pulse shaping is proposed for AFDM waveform. Some numerical results validate the coupling relationship of pulse shaping and the effectiveness of the proposed method in improving the channel sparsity and pilot-to-data interference.

## REFERENCES

- [1] R. Hadani, S. Rakib, M. Tsatsanis, A. Monk, A. J. Goldsmith, A. F. Molisch, and R. Calderbank, "Orthogonal time frequency space modulation," *IEEE WCNC*, San Francisco, CA, USA, Mar. 2017.
- [2] T. Thaj, E. Viterbo, and Y. Hong, "Orthogonal time sequency multiplexing modulation: analysis and low-complexity receiver design," *IEEE Trans. Wireless Commun.*, vol. 20, no. 12, pp. 7842-7855, Dec. 2021.
- [3] H. Lin and J. Yuan, "Orthogonal delay-doppler division multiplexing modulation," *IEEE Trans. Wireless Commun.*, vol. 21, no. 12, pp. 11024-11037, Dec. 2022.
- [4] Y. Chi, L. Liu, Y. Ge, X. Chen, Y. Li, and Z. Zhang, "Interleave frequency division multiplexing," *IEEE Wireless Commun. Lett.*, vol. 13, no. 7, pp. 1963-1967, July 2024.
- [5] A. Bemani, N. Ksairi, and M. Kountouris, "Affine frequency division multiplexing for next generation wireless communications," *IEEE Trans. Wireless Commun.*, vol. 22, no. 11, pp. 8214-8229, Nov. 2023.
- [6] Y. Zhou, C. Zou, N. Zhou, Y. Tang, X. Zhang, H. Yin, X. Liu, R. He, P. Tang, W. Yuan, and Y. Zeng, "Affine frequency division multiplexing for communication and channel sounding," *IEEE Veh. Technol. Mag.*, early access, DOI:10.1109/MVT.2025.3623786.
- [7] H. Yin, Y. Tang, A. Bemani, M. Kountouris, Y. Zhou, X. Zhang, Y. Liu, G. Chen, K. Yang, F. Liu, C. Masouros, S. Li, G. Caire, and P. Xiao, "Affine frequency division multiplexing: extending OFDM for scenario-flexibility and resilience," *IEEE Wireless Commun.*, early access, DOI:10.1109/MWC.2025.3600081.
- [8] H. Yin and Y. Tang, "Pilot aided channel estimation for AFDM in doubly dispersive channels," *IEEE/CIC Int. Conf. Commun. in China (ICCC)*, Sanshui, Foshan, China, Aug. 2022.

- [9] H. Yin, X. Wei, Y. Tang, and K. Yang, "Diagonally reconstructed channel estimation for MIMO-AFDM with inter-doppler interference in doubly selective channels," *IEEE Trans. Wireless Commun.*, vol. 23, no. 10, pp. 14066-14079, Oct. 2024.
- [10] C. Shen, J. Yuan, and J. Tong, "Time-domain zero-padding (TZP) AFDM with two-stage iterative MMSE detection," *IEEE Trans. Wireless Commun.*, early access, DOI:10.1109/TWC.2025.3624211.
- [11] H. Hawkins, C. Xu, L. Yang, and L. Hanzo, "Iterative Soft-MMSE Detection Aided AFDM and OTFS," *IEEE Open J. of Veh. Technol.*, vol. 6, pp. 2944-2959, Oct. 2025.
- [12] G. Liu, T. Mao, Y. Tang, J. Zhao, Z. Xiao, and Z. Han, "Multiple-mode affine frequency division multiplexing with index modulation," *IEEE Wireless Commun. Lett.*, early access, DOI:10.1109/LWC.2025.3621886.
- [13] Y. Tao, M. Wen, Y. Ge, T. Mao, Y. Tang, and A. Doosti-Aref, "Affine frequency division multiple access based on DAFT spreading for next-generation wireless networks," *IEEE Trans. Wireless Commun.*, early access, DOI: 10.1109/TWC.2025.3612880.
- [14] H. Yin, Y. Tang, S. Li, Y. Zhou, and C. Yi, "Evaluation and Design Criterion for Pulse-shaped AFDM," *IEEE GLOBECOM 2024*, Cape Town, South Africa, Dec 2024.